Article

Cancer Cell

Metabolic Inflammation-Associated IL-17A Causes Non-alcoholic Steatohepatitis and Hepatocellular Carcinoma

Graphical Abstract

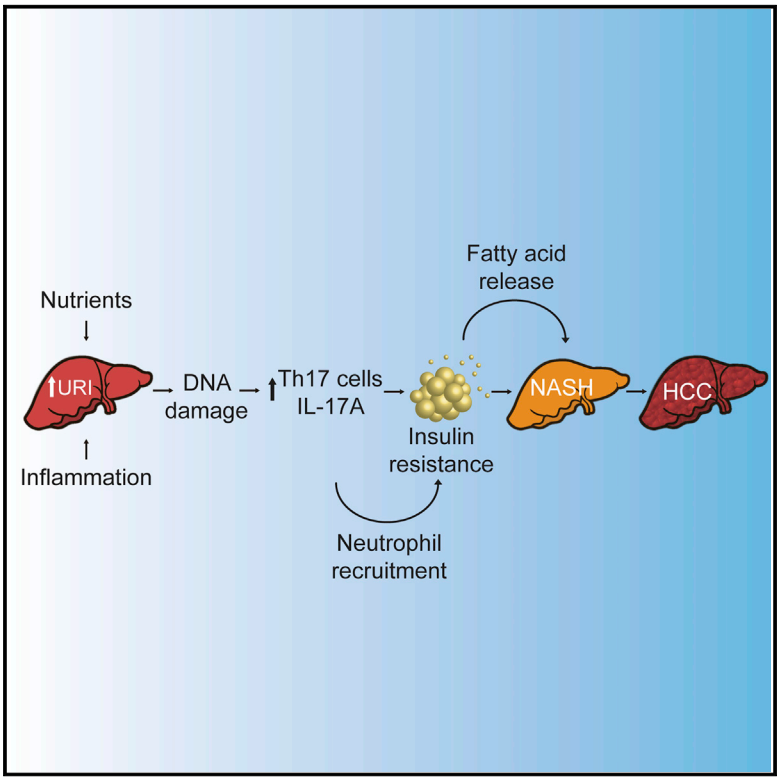

Authors

Ana L. Gomes, Ana Teijeiro, Stefan Burén, ..., Jean-Philippe Theurillat, Cristian Perna, Nabil Djouder

Correspondence

ndjouder@cnio.es

In Brief

Gomes et al. show that excess nutrients lead to URI-dependent DNA damage in hepatocytes, triggering inflammation via Th17 cells and IL-17A. Suppression of Th17 cell differentiation or blocking IL-17A signaling prevents non-alcoholic steatohepatitis and subsequent hepatocellular carcinoma.

Highlights

- Hepatic DNA damage triggers Th17 cell infiltration in the liver
- Hepatic Th17 cells and IL-17A production mediate WAT IR, NASH, and HCC
- Blocking IL-17A axis restores insulin sensitivity and prevents NASH and HCC
- IL-17A is high in human hepatitis, fatty livers, and viral hepatitis-associated HCC

Gomes et al., 2016, Cancer Cell *30*, 161–175
July 11, 2016
http://dx.doi.org/10.1016/j.ccell.2016.05.020

CellPress

Cancer Cell
Article

Metabolic Inflammation-Associated IL-17A Causes Non-alcoholic Steatohepatitis and Hepatocellular Carcinoma

Ana L. Gomes,[1,5] Ana Teijeiro,[1,5] Stefan Burén,[1] Krishna S. Tummala,[1] Mahmut Yilmaz,[1] Ari Waisman,[2] Jean-Philippe Theurillat,[3] Cristian Perna,[4] and Nabil Djouder[1,*]
[1]Cancer Cell Biology Programme, Growth Factors, Nutrients and Cancer Group, Centro Nacional de Investigaciones Oncológicas, CNIO, Madrid 28029, Spain
[2]Institute for Molecular Medicine, University Medical Center, Johannes Gutenberg University of Mainz, Mainz 55131, Germany
[3]Functional Cancer Genomics Group, Institute of Oncology Research (IOR), Bellinzona 6500, Switzerland
[4]Department of Pathology, Hospital Universitario Ramón y Cajal, IRYCIS, Madrid 28034, Spain
[5]Co-first author
*Correspondence: ndjouder@cnio.es
http://dx.doi.org/10.1016/j.ccell.2016.05.020

SUMMARY

Obesity increases hepatocellular carcinoma (HCC) risks via unknown mediators. We report that hepatic unconventional prefoldin RPB5 interactor (URI) couples nutrient surpluses to inflammation and non-alcoholic steatohepatitis (NASH), a common cause of HCC. URI-induced DNA damage in hepatocytes triggers inflammation via T helper 17 (Th17) lymphocytes and interleukin 17A (IL-17A). This induces white adipose tissue neutrophil infiltration mediating insulin resistance (IR) and fatty acid release, stored in liver as triglycerides, causing NASH. NASH and subsequently HCC are prevented by pharmacological suppression of Th17 cell differentiation, IL-17A blocking antibodies, and genetic ablation of the IL-17A receptor in myeloid cells. Human hepatitis, fatty liver, and viral hepatitis-associated HCC exhibit increased IL-17A correlating positively with steatosis. IL-17A blockers may prevent IR, NASH, and HCC in high-risk patients.

INTRODUCTION

Hepatocellular carcinoma (HCC) is a major cause of cancer-related death (Tummala et al., 2014). Risk factors include toxin poisoning, chronic alcohol consumption, chronic hepatitis virus B or C (HBV or HCV, respectively) infection, or chronic overfeeding and/or sedentary lifestyle-associated obesity, which promote non-alcoholic fatty liver disease (NAFLD), a condition characterized by excessive hepatocellular lipid accumulation (steatosis) (Marengo et al., 2016). NAFLD is highly prevalent among individuals who are obese or with diabetes or hyperlipidemia (Marengo et al., 2016). Hepatic steatosis combined with chronic inflammation and liver injury-associated fibrosis causes non-alcoholic steatohepatitis (NASH), the most severe form of NAFLD and a potential precursor of HCC (Marengo et al., 2016). HCC incidence is thus likely to increase with the pandemic spread of obesity. NASH, which is currently untreatable, is therefore a serious public health problem.

The exact pathogenesis of NASH is not clear. The ''two-hit'' model suggests that after a first hit (i.e., hepatic steatosis), a second hit (e.g., oxidative stress or cytokines) is needed to develop NASH (Day and James, 1998). Recently, multiple studies suggest that inflammation precedes steatosis in NASH (Wolf et al., 2014; Zhao et al., 2015). Steatosis per se may thus not account for the negative outcome of NASH, but inflammation determines the long-term prognosis of the disease (Tilg and Moschen, 2010). Several pro-inflammatory cytokines are reportedly implicated in hepatic steatosis and HCC (He et al., 2010; Park et al., 2010; Wolf

Significance

Obesity-induced NASH is a potent risk factor for HCC. HCC incidence is thus likely to increase with the pandemic spread of obesity and without therapeutic options, putting NASH in an alarming situation and a serious public health problem. We demonstrate that nutrient excess-induced URI expression triggers DNA damage. Upon genotoxic stress Th17 cells are triggered to the liver, inducing IL-17A production and subsequently WAT neutrophil recruitment, IR, NASH, and HCC. Therefore, inflammation precedes hepatic steatosis, and IR represents a risk factor for NASH, putting diabetic patients at high risk of developing hepatic disorders and HCC. IL-17A signaling blockers (e.g., digoxin) may be efficiently, inexpensively, and quickly transitioned to the clinic to prevent IR, NASH, and HCC, particularly in high-risk patients.

et al., 2014). Recent findings have determined interleukin 17A (IL-17A) in NAFLD pathogenesis (Harley et al., 2014), but in this context its cellular source, its mechanistic role in NASH and HCC, as well as the critical cell type and immune cells infiltrating the liver remain unknown.

Excessive hepatic fat accumulation in obese individuals is a robust marker of various metabolic abnormalities associated with insulin resistance (IR), diabetes, and dyslipidemia, and predisposes sufferers to NASH and HCC (Nagle et al., 2009; Perry et al., 2014). Inflammation reportedly induces IR in obese individuals, possibly because nutrient surpluses may lead to infiltration of immune cells into the liver and white adipose tissue (WAT). Accordingly, several inflammatory factors associated with metabolic changes link nutrient overload, IR and type 2 diabetes (T2D) (Donath et al., 2008; Gregor and Hotamisligil, 2011; Mraz and Haluzik, 2014; Patel et al., 2013; Talukdar et al., 2012). However, mechanisms of nutrient excess-associated NAFLD are not well understood. Moreover, it remains unknown how nutrient excesses induce immune responses and how immune cells link WAT to metabolic dysfunctions leading to HCC. It is also unclear whether NAFLD is a cause or a consequence of metabolic dysfunctions. A better understanding of the mechanisms responsible for the pathogenesis and pathophysiology of NAFLD may identify biomarkers for metabolic risk and therapeutic approaches for NASH and HCC.

Prospective data and epidemiological studies are needed to clarify the progression from NAFLD to HCC. Genetic mouse models mimicking different stages of human hepatocarcinogenesis would help to mechanistically understand NASH development and progression. We investigate here the molecular mechanisms linking nutrient surpluses and inflammation to NASH and HCC.

RESULTS

URI Is Essential for NASH

We recently demonstrated that hepatic unconventional prefoldin RPB5 interactor (URI) expression in mouse induces multistep HCC that encompassed the HBV-associated human HCC signature. In particular, URI expression in mouse and human livers was modulated by viral infections and inflammatory cues (Tummala et al., 2014). To explore whether excessive nutrients also modulate hepatic URI level that may link it to NASH and HCC, we fed C57BL/6 mice for 1 month with various NASH diets that may promote HCC (Takahashi et al., 2012; Wolf et al., 2014). High-fat-diet (HFD)-fed mice exhibited increased body weight, liver weight, and hepatic URI levels, whereas hepatic URI expression fell in mice starved for 16 hr (Figures 1A and 1B). URI was also upregulated in livers of mice fed with the methionine- and choline-deficient (MCD)-HFD (Figure 1C). However, these mice had a significant decrease in body and liver weights (Figure 1D). We thus used a choline-deficient (CD)-HFD, which recapitulates key features of human NASH (Wolf et al., 2014). C57BL/6 mice fed with CD-HFD exhibited increased hepatic URI levels and body weight, but no differences were observed in liver weight (Figures 1C and 1D). Thus, hepatic URI can potentially link metabolic surpluses to NASH and HCC.

Homozygous deletion of URI in hepatocytes (URI(Δ/Δ)^{hep}) leads to death of mice at around 1 week but heterozygous (URI(+/Δ)^{hep}) mice are viable (Tummala et al., 2014). HFD-fed URI(+/Δ)^{hep} mice and wild-type (WT) littermates had similar body and liver weights at 32 weeks (Figure S1A). However, HFD-fed URI(+/Δ)^{hep} mice exhibited significantly less hepatic lipid accumulation as shown by H&E, oil red O (ORO) staining, and hepatic triglyceride (TG) determination (Figures 1E–1G). Importantly, CD-HFD- or MCD-HFD-fed URI(+/Δ)^{hep} mice also showed decreased hepatosteatosis (Figures 1H–1J). Thus, hepatic URI may be essential in NAFLD.

We also used a knockin mouse, hURI-tetOFF^{hep}, whose hepatocytes express human URI (hURI) (Tummala et al., 2014). The model exhibits multistep HCC-dependent genotoxic stress with the appearance of spontaneous HCCs by 65 weeks of age (Tummala et al., 2014). WT littermates and hURI-tetOFF^{hep} mice are hereafter referred to as "controls" and "mutants," respectively. Chow-fed mutants spontaneously developed classical histological features of human steatohepatitis at 32 weeks including hepatocyte ballooning, Mallory-Denk bodies, and micro- and macro-steatosis (Figures S1B–S1D). When hURI expression was disabled by feeding 8-week-old mutants with a doxycycline diet, analysis at 32 weeks revealed no differences of lipid accumulation between controls and mutants, despite a slight steatotic effect of doxycycline (Figures S1B–S1E) (Deboyser et al., 1989). Blocking hURI expression did not affect liver weight and restored normal body mass (Figures S1F and S1G). Thus, continuous hepatic URI expression seems necessary for sustained hepatosteatosis.

Next, we checked for other features of NASH. HFD-fed URI(+/Δ)^{hep} mice showed decreased Sirius red (SR) staining and alanine aminotransferase (ALT) levels than their littermates (Figures 1E, 1K, and 1L), indicating less fibrosis and liver injury. Notably, no biliary damage was detected as shown by direct bilirubin (Figure S1H). CD-HFD- or MCD-HFD-fed URI(+/Δ)^{hep} mice also exhibited less fibrosis (Figures 1H, 1M, and 1N). Importantly, 32-week-old mutants had enhanced liver injury (Figures S1B, S1I, and S1J), but serum bilirubin levels were not affected (Figure S1K). Blocking hURI expression prevented liver damage (Figures S1B, S1I, and S1J). Notably, doxycycline induced liver injury (Figure S1J), as previously reported (Bjornsson et al., 1997). Thus, hepatic URI is apparently important for chronic liver injury.

Intriguingly, there were no differences in hepatic F4/80^{+} macrophages or CD3ε^{+} T cell infiltration in HFD-fed URI(+/Δ)^{hep} mice compared with their WT littermates, but HFD increased inflammatory cell levels in all mice (Figures 1E, S1L, and S1M). Notably, mutant hURI-tetOFF^{hep} livers showed enhanced macrophages and T cells (Figures S1B, S1N, and S1O). Among increased macrophages in mutants, M2 macrophages (F4/80^{+}Cd206^{+}Cd11c^{-}) were enhanced, but not the M1 population (F4/80^{+}Cd11c^{+} Cd206^{-}) (Figure S1P). Ly6C^{hi} monocyte counts were similar to those of controls (Figures S1Q and S1R), suggesting that hepatic macrophages are Kupffer cells but may not be bone marrow-derived macrophages. Disabling hURI expression prevented inflammatory cell infiltration (Figures S1B, S1N, and S1O). Expressing hURI from adult stage (8 weeks) demonstrated that steatohepatitis is independent of embryonic development (Figures S1S–S1Y). Therefore, hepatic URI is critical for steatohepatitis.

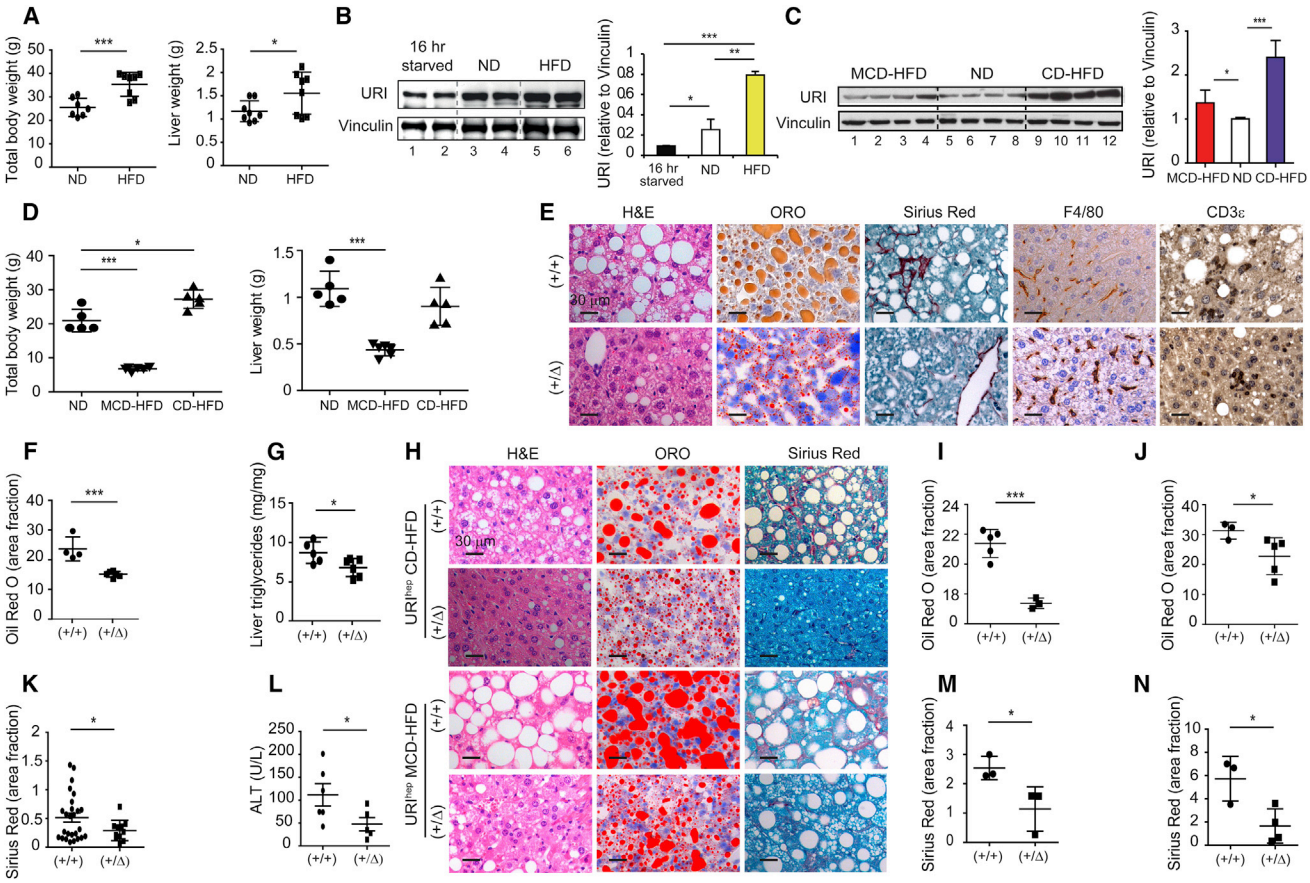

Figure 1. URI Is Essential for NASH

(A) Body and liver weights of C57BL/6 mice under ND or HFD since 8 weeks of age for 1 month ($n \geq 7$).

(B) WB and quantification of URI of livers from mice described in (A), with vinculin used as a loading control ($n = 2$).

(C) WB and quantification of URI of livers from C57BL/6 mice under MCD-HFD, ND, or CD-HFD since weaning for 1 month ($n = 4$).

(D) Body and liver weights of mice described in (C) ($n \geq 5$).

(E) Staining and IHC of livers from 32-week-old URI(+/+)^{hep} and URI(+/Δ)^{hep} mice under HFD since 8 weeks of age ($n \geq 5$).

(F and G) Quantification of hepatic ORO (F) and TGs (G) from mice described in (E) ($n \geq 5$).

(H) Staining and IHC of livers from 28-week-old URI(+/+)^{hep} and URI(+/Δ)^{hep} mice under CD-HFD or MCD-HFD for 6 and 4 weeks, respectively ($n \geq 3$).

(I and J) Quantification of hepatic ORO from 28-week-old URI(+/+)^{hep} and URI(+/Δ)^{hep} mice under CD-HFD (I) or MCD-HFD (J) for 6 and 4 weeks, respectively ($n \geq 3$).

(K) SR quantification from (E) ($n \geq 11$).

(L) ALT from mice described in (E) ($n \geq 5$).

(M and N) SR quantification from mice described in (I) and (J), respectively ($n \geq 3$).

Statistical analysis was performed using unpaired two-tailed Student's t test or unpaired t test with Welch's correction in (K). Data are represented as means ± SD. *$p \leq 0.05$, **$p \leq 0.01$, ***$p \leq 0.001$. See also Figure S1.

Hepatic URI Expression-Mediated IR in WAT Causes NASH

Next, we checked whether increased steatosis in mutants hURI-tetOFF^{hep} resulted from de novo lipid synthesis or free fatty acid (FFA) uptake by the liver (Nagle et al., 2009). Mutants exhibited reduced hepatic mRNA levels of de novo lipid synthesis enzymes such as sterol regulatory element-binding protein 1c, fatty acid synthase (FAS), ATP citrate lyase, and acetyl-coenzyme A carboxylase (Figure S2A). Western blotting (WB) confirmed that FAS levels were reduced in mutants, but remained unchanged in URI(+/Δ)^{hep} mice compared with their WT littermates (Figure S2B). Mutants also exhibited elevated mRNA and protein levels of peroxisome proliferator-activated receptor γ (PPARγ), which is implicated in lipid uptake (Figures S2A and S2B). Similarly, the scavenger receptor CD36 (a fatty acid [FA] transporter) was downregulated in URI(+/Δ)^{hep} mice but upregulated in mutants (Figure S2B), suggesting a FFA uptake alteration in URI mice. Serum FFA and blood diacylglycerol (DAG) levels were significantly reduced in HFD-fed URI(+/Δ)^{hep} (Figures 2A and 2B) but increased in mutants (Figures S2C and S2D). Suppressing hURI expression abolished FFA increases in mutants (Figure S2C). Thus, URI-induced hepatic steatosis is probably caused by FFA uptake rather than de novo synthesis.

Hepatic fat is mainly deposited as TGs, formed from circulating FAs mobilized via lipolysis from WAT and stored as lipid droplets within hepatocytes (Nagle et al., 2009). FFA increases

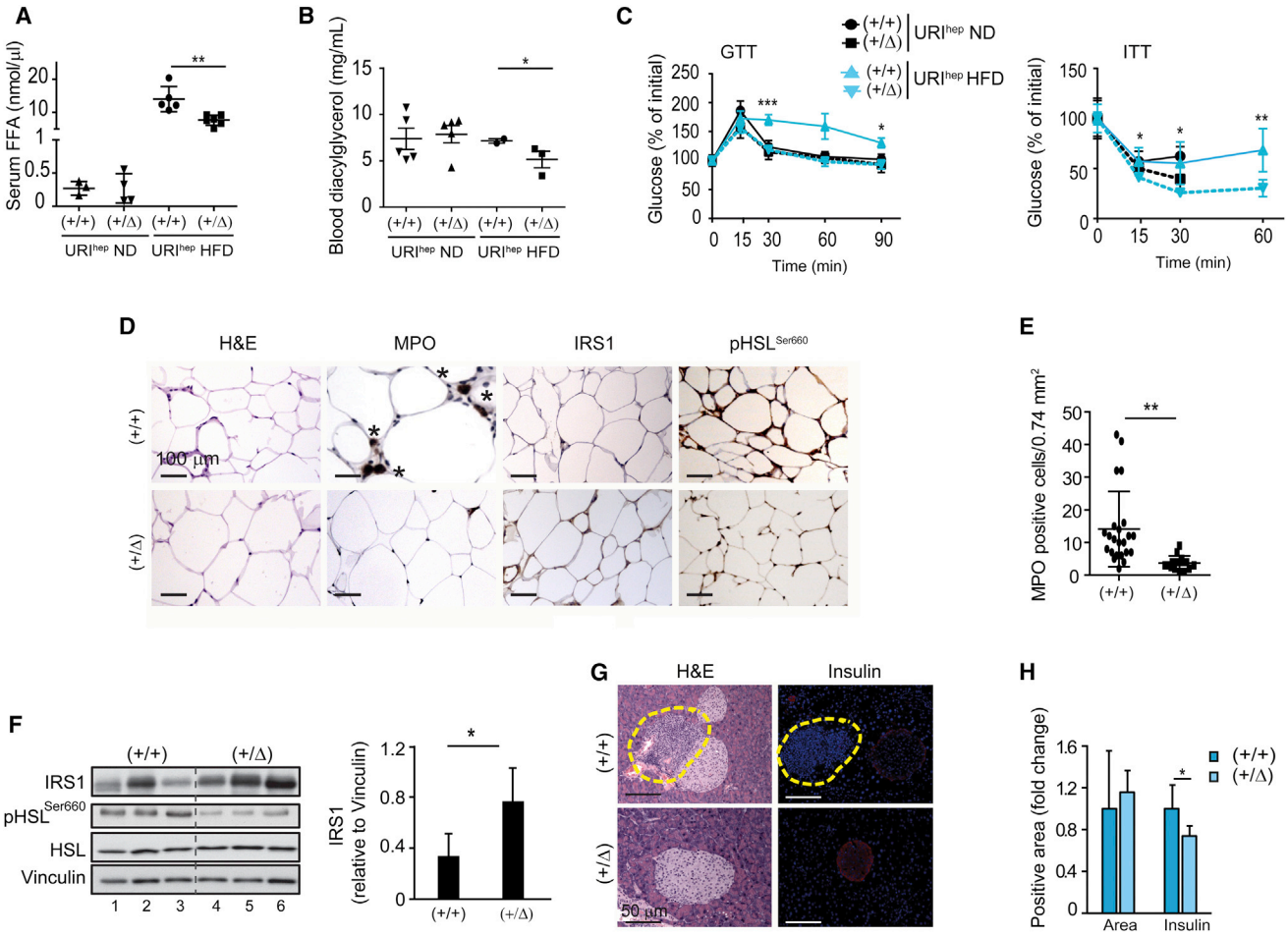

Figure 2. Hepatic URI Expression-Mediated IR in WAT Causes NASH

(A and B) FFA (A) and DAG (B) in 32-week-old URI(+/+)^{hep} and URI(+/Δ)^{hep} mice under ND or HFD since 8 weeks of age (n ≥ 3).

(C) GTT and ITT in mice described in (A) (n ≥ 3).

(D) Staining and IHC of WAT from 32-week-old URI(+/+)^{hep} and URI(+/Δ)^{hep} mice under HFD since 8 weeks of age (n ≥ 6). Asterisks denote MPO^{+} cells.

(E) MPO quantification from (D) (n ≥ 13).

(F) WB of WAT and quantification of IRS1 from mice described in (D) (n = 3).

(G) Staining of pancreas from mice described in (D) (n ≥ 4). Yellow circles denote intra-islet inflammation.

(H) Quantification of islet size (area fraction) and insulin-positive area per islet in (G).

Statistical analysis was performed using unpaired two-tailed Student's t test. Data are represented as means ± SD. *p ≤ 0.05, **p ≤ 0.01, ***p ≤ 0.001. See also Figure S2.

are thus possibly due to IR-mediated WAT lipolysis. Densitometry revealed that mutants had significantly less body fat, and disabling hURI expression prevented fat loss in mutants (Figure S2E). Moreover, glucose and insulin tolerance tests (GTT and ITT, respectively) revealed that genetic URI reduction protected against HFD-induced glucose intolerance and IR (Figure 2C). Importantly, impaired glucose tolerance and insulin sensitivity were detected in mutants, but could be relieved by suppressing hURI expression (Figure S2F), suggesting that WAT IR requires sustained hepatic hURI expression. Finally, mutants exhibited increased blood insulin and adipokines (Figure S2G), with decreased adiponectin levels (Figure S2H), indicating perturbation of glucose homeostasis. WAT IR thus promotes lipolysis and FFA release, and may consequently induce hepatosteatosis in URI mice.

Among inflammatory infiltrates, neutrophils and neutrophil-secreted elastase reportedly induce WAT IR (Talukdar et al., 2012). Myeloperoxidase (MPO) staining showed that neutrophil infiltration into WAT was significantly reduced in HFD-fed URI(+/Δ)^{hep} mice (Figures 2D and 2E). Mutants' WAT had high levels of neutrophils but was almost undetectable after blocking hURI expression in mutants (Figures S2I and S2J). Notably, macrophages were neither increased nor activated in mutants' WAT (Figures S2K–S2M). Hepatic URI is thus essential for neutrophil infiltration into WAT.

HFD-fed URI(+/Δ)^{hep} mice exhibited significantly increased IRS1 levels and decreased activating phosphorylation of the lipolytic enzyme hormone-sensitive lipase (HSL) at Ser-660 (which hydrolyses stored TGs into FFA) (Figures 2D and 2F). Conversely, mutants' WAT revealed decreased insulin receptor

substrate 1 (IRS1) levels, consistent with elastase-mediated IRS1 degradation and IR (Talukdar et al., 2012), and increased HSL Ser-660 phosphorylation (Figures S2I and S2N). Thus, hepatocytic URI may induce NASH via WAT IR and increased lipolysis.

In pre-diabetic individuals, chronic low-grade systemic WAT and pancreatic inflammation induces compensatory increases in the mass and insulin content of β cells with subsequent β cell exhaustion and T2D (Donath et al., 2008). Interestingly, 32-week-old mutants showed basal glucose levels identical to those of controls but failed to reduce glucose levels upon fasting (Figure S2O), suggesting a pre-diabetic state. H&E staining of mutant's pancreas revealed intra-islet inflammation and vascular dilation (Figure S2P), classical features of human T2D, demonstrating that systemic inflammation affects mutants' pancreases. Mutants' β cells also had greater masses and insulin contents than those of controls (Figures S2P and S2Q). These features mimic human IR/T2D and indicate that chronic URI expression in hepatocytes induces systemic low-grade chronic inflammation and IR in WAT, which is implicated in NASH. Conversely, URI $(+/\Delta)^{hep}$ mice were protected against HFD-induced pancreatic inflammatory infiltration and displayed less insulin content (Figures 2G and 2H).

Hepatic URI Expression Induces DNA Damage, and Triggers Hepatic T Cell Infiltration and Increased IL-17A

Although no inflammation is detected during early stages of hURI expression (3 weeks of age), hepatocarcinogenesis is induced by genotoxic stress, an early event (Tummala et al., 2014), suggesting that hepatic DNA damage precedes inflammation in mutant hURI-tetOFF^{hep} mice. Interestingly, livers from 8-week-old mutants showed an increase in T cells and Kupffer cells (Figures 3A and 3B) with a decrease in B cell number (Figures S3A and S3B) and unchanged counts of mast cells (not shown). A diet containing nicotinamide riboside (NR), which prevents DNA damage (Tummala et al., 2014), abolished inflammatory cell infiltration in 8-week-old mutants (Figures 3A and 3B). Importantly, hepatic DNA damage and inflammation were enhanced in HFD-fed C57BL/6 and significantly reduced in NR-treated mice (Figures 3C–3E). HFD-fed URI$(+/+)^{hep}$ mice also increased DNA damage, which was reduced upon URI depletion (Figure 3F). Thus, HFD increases URI-inducing genotoxic stress to trigger metabolic inflammation (perhaps via apoptosis) during the early stages of NASH. Nutrient overload, somehow mimicked by hepatic URI expression, is a genotoxic stress model.

Early blood cytokine profiling of 8-week-old mutants revealed elevated levels of IL-17A and keratinocyte chemoattractant, both implicated in neutrophil recruitment (Sadik et al., 2011), and modestly elevated levels of tumor necrosis factor α, which reportedly influences progression of NASH to HCC (Figure 3G) (Park et al., 2010). Notably, only IL-17A and granulocyte-colony stimulating factor (G-CSF), a neutrophil-recruiting protein whose expression is induced by IL-17A, remained elevated in 32-week-old mutants (Figure 3H) (Fossiez et al., 1996), suggesting that chronic hepatic hURI expression induces systemic inflammation that may depend on IL-17A. Accordingly, a hemogram showed that 32-week-old mutants exhibited leukocytosis, especially lymphocytosis and granulocytosis, but no significant changes in minimum inhibitory dilution cells were observed (Figure 3I). Elevated IL-17A levels and the expression of IL-17A target lipocalin 2 (*Lcn2*) were also observed in 32-week-old mutants' livers or WAT (Figures 3J–3L). As seen for URI, increased IL-17A was also observed in livers of HFD-, CD-HFD-, or MCD-HFD-fed C57BL/6 mice (Figures 3M and 3N). Importantly, reduced levels of IL-17A and granulocyte-macrophage CSF (GM-CSF) were detected in HFD-fed URI$(+/\Delta)^{hep}$ mice (Figure 3O).

WB in livers revealed that activation of some potential targets of the IL-23/IL-17A axis (ERK, GSK3β, JNK, STAT3) was reduced in HFD-fed URI$(+/\Delta)^{hep}$ mice while being increased in mutants (Figure S3C). Phosphorylation of p38 as well as β-catenin levels were not affected, but p65 levels were apparently augmented in some liver inflammatory cells when URI was expressed in hepatocytes (Figures S3C and S3D), suggesting that URI expression may control the IL-23/IL-17A pathway. Thus, hepatocytic URI induces DNA damage, triggering early hepatic T cell infiltration and IL-17A release, which may be the early immune effectors in systemic inflammation, neutrophil activation, and NASH-associated WAT IR pathogenesis.

Th17 Cells Mediate WAT IR, NASH, and HCC

Flow cytometry analysis of HFD-fed URI $(+/\Delta)^{hep}$ mice showed no differences in T cells ($CD3\varepsilon^+$) in livers and blood, consistent with CD3ε staining (Figures 1E and S1M). However, liver and circulating IL-17A-expressing T helper (Th) 17 cells ($CD3^+CD4^+CD8^-$IL-$17A^+$) were significantly reduced, even though no differences were observed in other $CD3\varepsilon^+$ subpopulations, including Th cells ($CD3^+CD4^+CD8^-$), T cytotoxic (Tc) cells ($CD3^+CD4^-CD8^+$), and γδT cells ($CD3^+CD4^-CD8^-\alpha\beta$ $TCR^-\gamma\delta$ TCR^+) (Figures 4A and S4A).

Importantly, cells positive for the RAR-related orphan receptor γt (RORγt), a transcription factor promoting Th17 cell differentiation, were increased upon HFD and decreased with URI deletion (Figure S4B). Moreover, 8-week-old C57BL/6 mice fed with HFD for 4 weeks, which leads to URI expression and DNA damage, exhibited increases in circulating Th17 cells (Figures 4B and S4C). Thus, HFD may increase the overall level of T cells (via DNA damage) but URI may contribute specifically to the increase in Th17 cells. Accordingly, T, Th, and Th17 cells were significantly increased in mutants but γδT or Tc cells were not affected (Figures 4C and S4D–S4F). Therefore, hepatocytic URI expression induces systemic inflammation that may be orchestrated by Th17 cells at early stages of NASH-induced HCC.

Digoxin inhibits RORγt transcriptional activity to suppress Th17 cell differentiation without affecting differentiation of other T cells (Huh et al., 2011). Flow cytometry analysis showed that treating mutants with digoxin reduced levels of circulating Th17 cells and serum IL-17A (Figures 4C, S4G, and S4H). A hemogram revealed that digoxin prevented hURI-induced lymphocytosis and granulocytosis (Figure S4I). Importantly, at 32 weeks reduced levels of hepatosteatosis in digoxin-treated mutants were detected (Figures 4D and 4E). Digoxin treatment also reduced hepatic immune cell infiltration and liver injury (Figures 4D and 4F–4H). Moreover, 32-week-old digoxin-treated mutants exhibited greater glucose tolerance and insulin sensitivity than non-treated mice, with increased IRS1 levels and reduced MPO, HSL phosphorylation, elastase, and IL-17A levels in WAT (Figures 4I–4L). The restoration of insulin sensitivity was

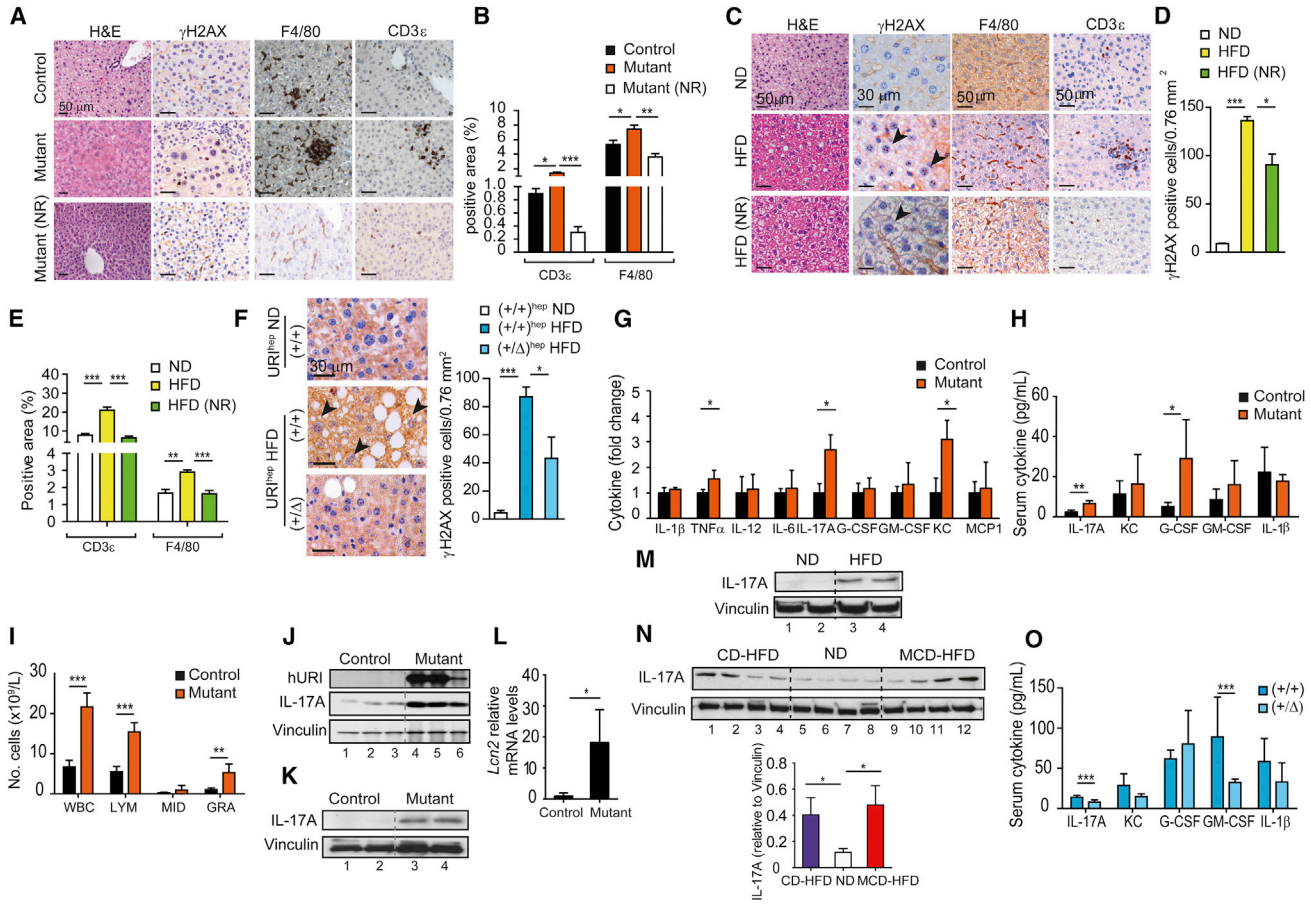

Figure 3. Hepatic URI Expression Induces DNA Damage, and Triggers Hepatic T Cell Infiltration and Increased IL-17A

(A) Staining and IHC of livers from 8-week-old hURI-tetOFF^{hep} mice under ND or NR diet since 3 weeks of age (n $\geq$ 4).

(B) CD3ε and F4/80 quantification from (A).

(C) Staining and IHC of livers from 8-week-old C57BL/6 mice under ND, HFD, or HFD with NR diet since 3 weeks of age (n $\geq$ 5). Arrowheads denote γH2AX$^+$ cells.

(D and E) γH2AX (D) and CD3ε and F4/80 (E) quantification from (C).

(F) γH2AX IHC and quantification in livers from 32-week-old URI^{hep} mice under ND or HFD since 8 weeks of age (n $\geq$ 4). Arrowheads denote γH2AX$^+$ cells.

(G and H) Circulating cytokines in 8-week-old (G, n $\geq$ 4) and 32-week-old (H, n $\geq$ 6) hURI-tetOFF^{hep} mice.

(I) Hemogram of mice described in (H) (n $\geq$ 6).

(J and K) WB of livers (J, n = 3) and WAT (K, n = 2) from mice described in (H).

(L) qRT-PCR in livers from mice described in (H) (n $\geq$ 4).

(M) WB of livers from C57BL/6 mice under ND or HFD since 8 weeks of age for 1 month (n = 2).

(N) WB and quantification of IL-17A of livers from C57BL/6 mice under CD-HFD, ND, or MCD-HFD since 4 weeks of age for 1 month (n = 4).

(O) Circulating cytokines in 32-week-old URI(+/+)^{hep} and URI(+/Δ)^{hep} mice under HFD since 8 weeks of age (n $\geq$ 6).

Statistical analysis was performed using unpaired two-tailed Student's t test. Data are represented as means ± SD. *p $\leq$ 0.05, **p $\leq$ 0.01, ***p $\leq$ 0.001. See also Figure S3.

accompanied by decreased FFA and DAG levels (Figures 4M and S4J), indicating reduced lipolysis.

Importantly, digoxin significantly reduced dysplastic foci, known to be HCC precursors (He et al., 2013), and, thus, early-stage tumors (Figures S4K and S4L). Moreover, 65-week-old mutants, known to develop HCC (Tummala et al., 2014), exhibited no tumors when treated with digoxin (Figures 4N and 4O). For further characterization, resected tumors were analyzed by IHC using several markers currently used for clinical assessment of human HCC (Lo and Ng, 2013). Expression of heat shock protein 70 (HSP70), α-fetoprotein (AFP), glutamine synthetase (GS), cytokeratin 19 (CK19), and sex-determining region Y box (SRY box) containing gene 9 (Sox9) were used to stain liver tumors. GS and HSP70 have been shown to be useful for the diagnosis of malignant hepatocellular neoplasms (Di Tommaso et al., 2007). CK19 (Uenishi et al., 2003), Sox9 (Guo et al., 2012), and GS (Osada et al., 2000) are also reported in HCC diagnosis with bad prognosis. Finally, AFP is positively identified in one-third of HCCs, mainly in higher histological grades (Zhao et al., 2013). Based on their expression levels and previously reported classification, "HAGCS" (HSP70, AFP, GS, CK19, and Sox9) scores (in a.u.) were created to classify tumors' aggressiveness. Aggressive HCCs had the highest HAGCS scores, whereas HCAs scored lower in mutants (Figures 4P and S4M), suggesting that in addition to the histopathological characterization (Figure 4O), the HAGCS scores can be useful

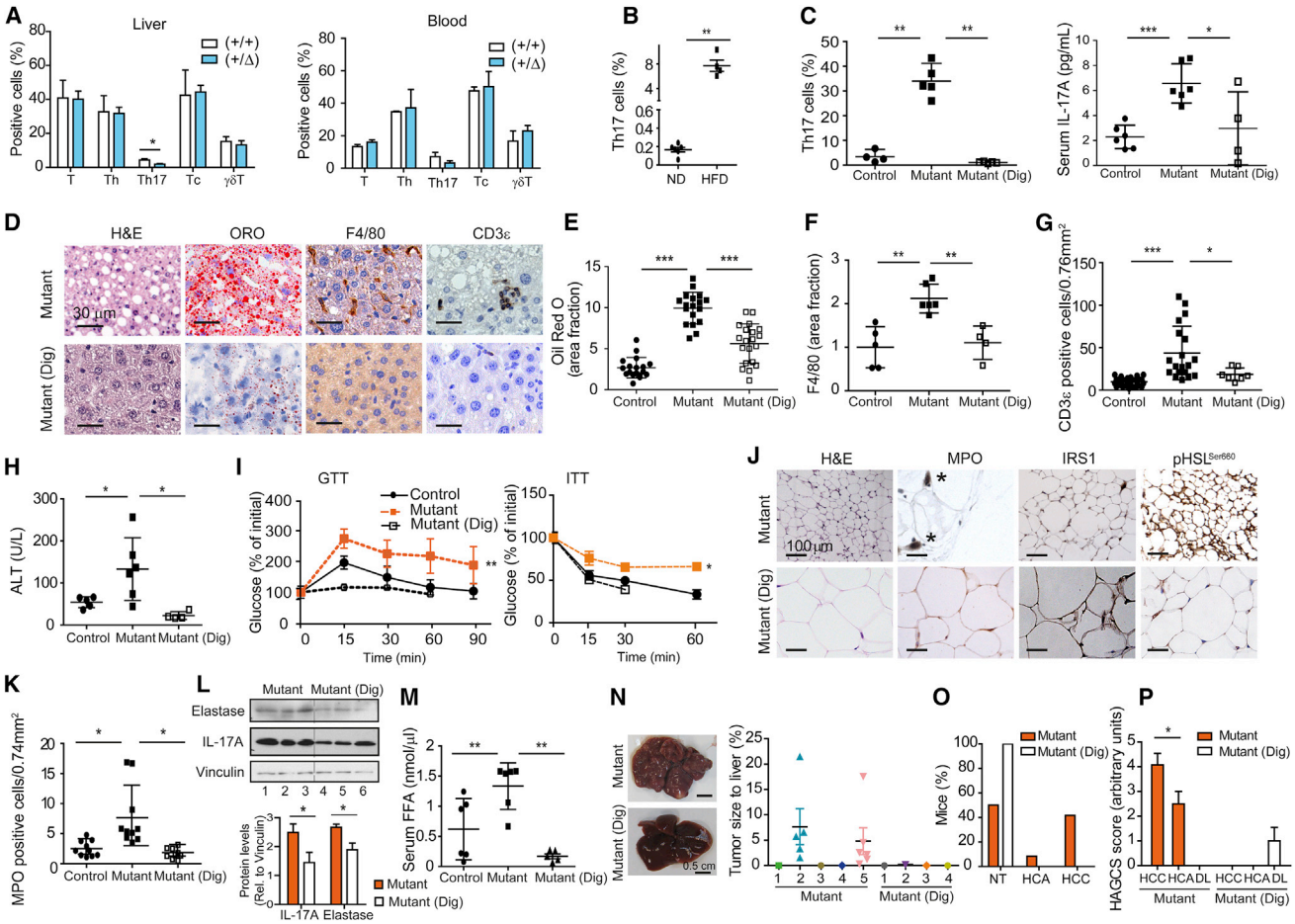

Figure 4. Th17 Cells Mediate WAT IR, NASH, and HCC

(A) Quantification of T cells in livers ($n \geq 5$) and blood ($n \geq 3$) from 32-week-old URI(+/+)^{hep} and URI(+/Δ)^{hep} mice under HFD since 8 weeks of age.

(B) Quantification Th17 cells in blood from C57BL/6 mice under ND or HFD since 8 weeks of age for 1 month ($n \geq 4$).

(C) Quantification of Th17 cells in blood and circulating IL-17A in 32-week-old hURI-tetOFF^{hep} mice with/without digoxin (Dig) since 8 weeks of age ($n \geq 4$).

(D) Staining and IHC of livers from mice described in (C) ($n \geq 6$).

(E–G) ORO (E), F4/80 (F), and CD3ε (G) quantification from (D) ($n \geq 4$).

(H) ALT in mice described in (C) ($n \geq 3$).

(I) GTT and ITT in mice described in (C) ($n \geq 3$).

(J) Staining and IHC of WAT from mice described in (C). Asterisks denote MPO^{+} cells ($n \geq 6$).

(K) MPO quantification from (J).

(L) WB and quantification of IL-17A and elastase of WAT from mice described in (C) (n = 3).

(M) FFA in mice described in (C) ($n \geq 5$).

(N) Representative liver pictures and quantification of tumoral area ($n \geq 4$) of 65-week-old hURI-tetOFF^{hep} mutant mice with/without Dig since 8 weeks of age.

(O) Percentage of mice described in (N) bearing liver abnormalities: no tumor (NT), adenoma (HCA), or HCC ($n \geq 5$).

(P) HAGCS score in mice described in (N) ($n \geq 5$). DL, dysplatic lesions.

Statistical analysis was performed using two-way ANOVA (I) or unpaired two-tailed Student's t test (A–C, E–H, K–M, and P). Data are represented as means ± SD. *$p \leq 0.05$, **$p \leq 0.01$, ***$p \leq 0.001$. See also Figure S4.

for clinical tumor assessment. Thus, hepatocytic URI-induced DNA damage recruits Th17 cells, mediating (possibly via IL-17A secretion) systemic inflammation, WAT IR, NASH, and HCC.

Diethylnitrosamine (DEN) in combination with HFD is reported to be a quicker model of obesity-induced HCC (Park et al., 2010). DEN-HFD-fed C57BL/6 mice increased IL-17A (Figure S4N), and thus were treated with digoxin (Figure S4O). Steatohepatitis, liver injury, neutrophil infiltration (MPO), and HSL activation were drastically reduced upon digoxin treatment (Figures S4P–S4U). Importantly, DEN-HFD-treated mice displayed tumors that were not apparent when treated with digoxin (Figure S4V), suggesting that inhibition of Th17 differentiation may prevent NASH-induced HCC.

Recombinant IL-17A Induces NASH in C57BL/6 Mice

We next tested whether recombinant IL-17A (rIL-17A) injection in chow-fed C57BL/6 mice would mimic WAT IR and NASH. As seen for the mutants, mice treated for 4 weeks with rIL-17A enhanced hepatic DNA damage and exhibited hepatosteatosis, increased hepatic TG levels, higher FFA levels, and lower body

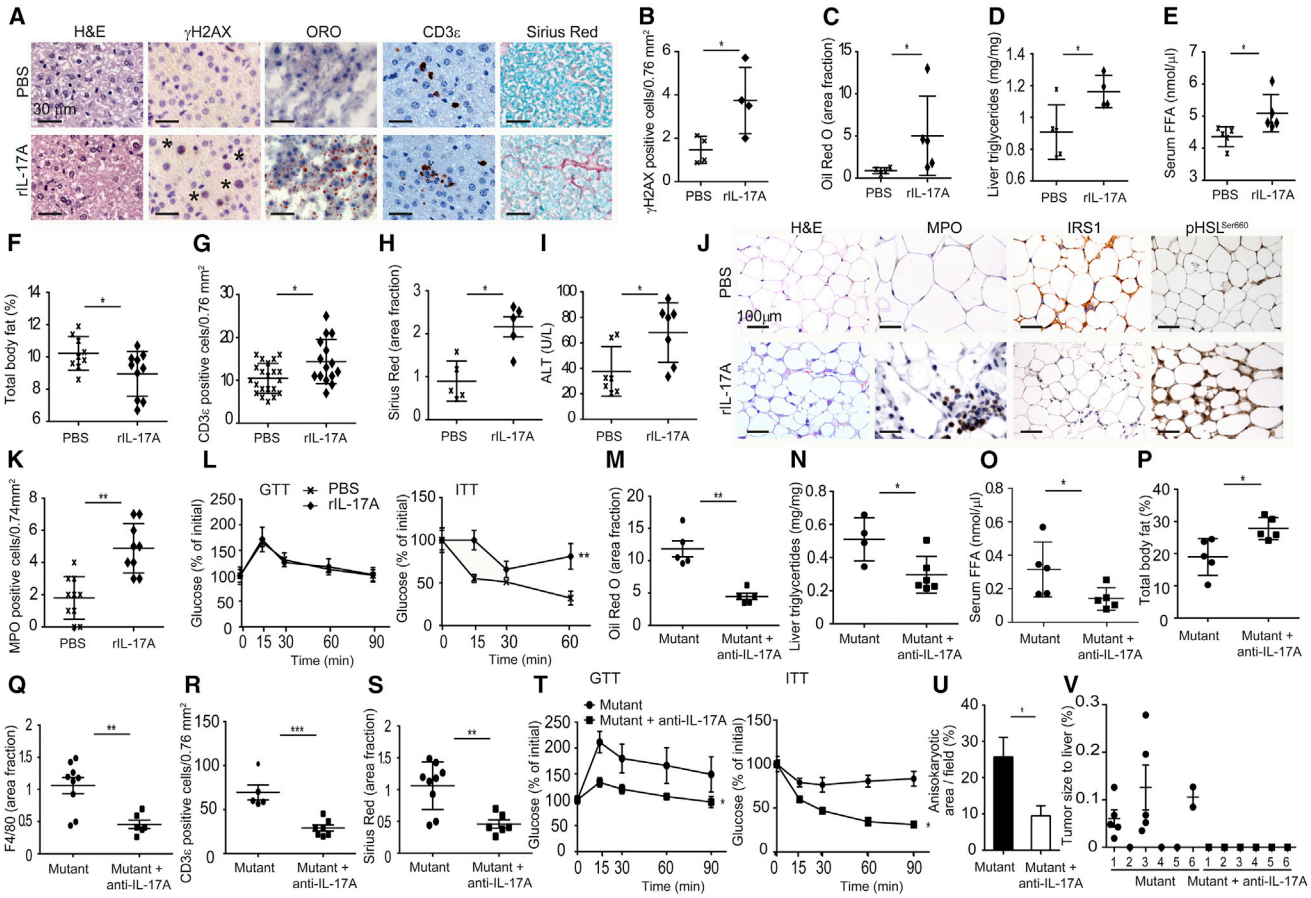

Figure 5. Recombinant IL-17A Induces NASH in C57BL/6 Mice, and Blocking IL-17A in Mutants Restores Insulin Sensitivity and Prevents NASH and HCC

(A) Staining and IHC of livers from 8-week-old C57BL/6 mice treated either with PBS or rIL-17A for 4 weeks ($n \geq 4$). Asterisks denote γH2AX$^+$ cells.

(B) γH2AX quantification from (A).

(C–E) Quantification of hepatic ORO (C), TG (D), and FFA (E) in mice described in (A) ($n \geq 4$).

(F) Percentage of body fat in mice described in (A) ($n \geq 4$).

(G and H) Quantification of CD3ε (G) and SR (H) from (A) ($n \geq 4$).

(I) ALT in mice described in (A) ($n \geq 4$).

(J) Staining and IHC of WAT from mice described in (A) ($n \geq 4$).

(K) MPO quantification from (J).

(L) GTT and ITT in mice described in (A) ($n \geq 4$).

(M and N) Quantification of hepatic ORO (M) and TG (N) from 32-week-old hURI-tetOFF^{hep} mice treated with/without anti-IL-17A ($n \geq 5$).

(O) FFA in mice described in (M) and (N) ($n \geq 5$).

(P) Percentage of body fat in mice described in (M) and (N) ($n \geq 5$).

(Q–S) Quantification of F4/80 (Q), CD3ε (R), and SR (S) from Figure S5J.

(T) GTT and ITT in mice described in (M) and (N) ($n \geq 5$).

(U) Quantification of anisokaryotic area in mice described in (M) and (N) ($n \geq 5$).

(V) Quantification of tumoral area in mice described in (M) and (N) ($n \geq 6$).

Statistical analysis was performed using two-way ANOVA (L and T) or unpaired two-tailed Student's t test (B–I, K, M–S, and U). Data are represented as means ± SD. *$p \leq 0.05$, **$p \leq 0.01$, ***$p \leq 0.001$. See also Figure S5.

fat (Figures 5A–5F and S5A) than C57BL/6 mice treated with vehicle. PPARγ was also increased in rIL-17A-treated animals (Figure S5B). Interestingly, hepatic URI was upregulated in these mice, possibly resulting from a positive feedback loop powering IL-17A effects and genotoxic stress (Figure S5B). Like mutants, these mice also had elevated levels of IL-17A and G-CSF (Figures S5B and S5C). Moreover, increased *Lcn2* expression and circulating Th17 cells were detected in rIL-17A-treated animals (Figures S5D–S5F). Notably, rIL-17A treatment specifically increased granulocytosis (Figure S5G) and T cell infiltration in the liver (Figures 5A and 5G). Furthermore, rIL-17A induced fibrosis and liver injury (Figures 5A, 5H, and 5I).

rIL-17A also increased WAT neutrophil infiltration and reduced IRS1 expression, promoting HSL activation (Figures 5J and 5K), all of which are consistent with WAT IR and lipolysis. It also

reduced insulin sensitivity without affecting glucose clearance (Figure 5L). Thus, rIL-17A induces characteristics observed in mutant and HFD-fed mice, suggesting that IL-17A is responsible for NASH via WAT IR.

Blocking IL-17A in Mutants Restores Insulin Sensitivity and Prevents NASH and HCC

We blocked IL-17A signaling in mutants using an antibody against IL-17A (Figure S5H). Blocking IL-17A in 32-week-old mutants reduced *Lcn2* expression (Figure S5I). This also significantly reduced hepatosteatosis and FFA, and increased body fat levels (Figures 5M–5P and S5J). In addition, lymphocytosis, granulocytosis, and hepatic Kupffer cell and T cell levels were significantly decreased (Figures 5Q, 5R, S5J, and S5K). Fibrosis was also prevented (Figures 5S and S5J). Furthermore, blocking IL-17A signaling in mutants hampered WAT neutrophil infiltration and lipolysis and restored WAT insulin signaling, improving glucose clearance and insulin sensitivity (Figures 5T and S5L).

Finally, while all mutants revealed high levels of dysplastic lesions and some developed early tumors at 32 weeks (Tummala et al., 2014), all mice with blocked IL-17A signaling exhibited reduced dysplastic foci and no tumors (Figures 5U, 5V, and S5M). IL-17A blockers could thus be useful for preventing metabolic dysfunction-associated HCC.

Genetic Ablation of IL-17RA in Myeloid Cells Blocks IL-17A Signaling and Suppresses HFD-Induced IR

IL-17A effects are mediated via a heterodimeric receptor comprising IL-17RA and IL-17RC (Korn et al., 2009). Mutants exhibited more IL-17RA^{+} granulocytes than controls (Figure 6A). IL-17A is reportedly a mediator of neutrophil recruitment (Miyamoto et al., 2003). In addition, pro-myelocytic cells (HL-60 and NB4) stimulated with rIL-17A showed activation of downstream signaling effectors (Figure S6A) and increased *LCN2* expression (Figure S6B), suggesting that myeloid cells may be directly activated by IL-17A. We therefore blocked IL-17A signaling by genetically ablating IL-17RA in myeloid cells through crossing *Il17ra*-flox (El Malki et al., 2013) and LysM-Cre mice (Clausen et al., 1999), generating offspring designated IL-17RA $(+/+)^{Myeloid}$ and IL-17RA $(\Delta/\Delta)^{Myeloid}$ (Figure 6B). HFD-fed IL-17RA $(\Delta/\Delta)^{Myeloid}$ mice exhibited no leukocytosis despite elevated IL-17A and Th17 levels (Figures 6C, 6D, S6C, and S6D), suggesting that IL-17A signaling via neutrophil activation may influence the onset of HFD-induced IR and NASH.

Hepatosteatosis was significantly reduced in HFD-fed IL-17RA $(\Delta/\Delta)^{Myeloid}$ mice (Figures 6E and 6F), which also had lower FFA levels and body fat than WT littermates (Figures 6G and 6H). Moreover, HFD-fed IL-17RA $(+/+)^{Myeloid}$ but not IL-17RA $(\Delta/\Delta)^{Myeloid}$ mice exhibited elevated ALT levels (Figure 6I). Notably, MCD-HFD-fed IL-17RA $(\Delta/\Delta)^{Myeloid}$ mice also had significantly less hepatosteatosis compared with IL-17RA $(+/+)^{Myeloid}$ mice (Figures S6E–S6H), and liver-infiltrating T cells were decreased (Figures S6F and S6I). HFD-fed IL-17RA $(+/+)^{Myeloid}$ mice also exhibited impaired glucose clearance and reduced insulin sensitivity relative to HFD-fed IL-17RA $(\Delta/\Delta)^{Myeloid}$ mice (Figure 6J). Finally, HFD-fed IL-17RA $(\Delta/\Delta)^{Myeloid}$ mice had fewer WAT-infiltrating neutrophils, increased levels of IRS1, and less HSL activation (Figure 6K). Thus, blocking IL-17A signaling in granulocytes protected against NASH diet-induced IR and steatohepatitis.

Genetic Ablation of IL-17RA in Myeloid Cells Alleviates IR, NASH, and HCC in Mutants

Next, IL-17RA $(\Delta/\Delta)^{Myeloid}$ mice were crossed with mutant mice. At 32 weeks of age hURI-tetOFF^{hep} mutants lacking IL-17RA in the myeloid compartment (hereafter termed "crosses") no longer presented signs of hepatosteatosis, and had higher body fat percentages (despite lower body weights and identical liver weights) and decreased FFAs (Figures 7A–7D, S7A, and S7B). Crosses had also reduced inflammation and ALT levels compared with the mutant mice (Figures 7A and 7E−7G). Thus, reducing IL-17A signaling may prevent NASH in URI mouse.

Although basal glucose levels in mutants and crosses were similar (Figure S7C), the crosses exhibited improved glucose clearance and enhanced insulin sensitivity (Figure 7H). In addition, crosses showed reduced MPO, increased IRS1 levels, and decreased HSL activation in WAT (Figure 7I). Therefore, IL-17A signaling accounts for the mutants' steatohepatitis and associated metabolic dysfunctions. Further, 32-week-old mutants had high dysplastic lesions and early liver tumors (Tummala et al., 2014), but the crosses did not (Figures S7D and S7E). Finally, 65-week-old mutants crossed with IL-17RA $(\Delta/\Delta)^{Myeloid}$ mice significantly reduced the number of aggressive HCCs (Figures 7J–7L and S7F). Thus, blocking IL-17A signaling may be useful for preventing NASH and HCC.

IL-17A Levels in Human Hepatitis, Human Fatty Livers, and Viral Hepatitis-Associated Human HCC Correlate Positively with Steatosis and URI Expression

To clarify our findings' clinical relevance, we examined URI and IL-17A expression in livers from obese individuals and peritumoral liver samples from non-obese patients. The former, but not the latter, exhibited high URI expression (Figure 8A). Although increased IL-17A was observed in fatty liver and peritumoral tissues, URI levels correlated positively with IL-17A protein and mRNA levels (Figures 8A–8C). Moreover, in human fatty livers, elevated IL-17A was detected only in CD4^{+} cells (Figure 8D) but not in HN4α^{+} hepatocytes (not shown). In addition, the number of IL-17A^{+} cells correlated with the steatotic state of the patients (Figure 8E). Importantly, increased hepatic TGs correlated positively with increased IL-17A mRNA levels (Figure 8F). Thus, in obese patients, hepatosteatosis is apparently associated with increased URI expression and high IL-17A levels.

IL-17A (confined in inflammatory cells) was also present in human viral hepatitis samples (mainly positive for URI expression), an early stage of HCC, and correlated with the steatotic state of these samples, suggesting that in human, IL-17A may initiate steatohepatitis progressing to HCC (Figures 8G–8I). Stratification of the data indicated that all HCV-infected patients with steatosis had URI expression, while only half of non-steatotic HCV patients exhibited URI expression (Figure 8J). Thus, URI expression correlates with NASH patients infected with hepatitis viruses.

Since URI is positively associated with HBV and HCV infection in human HCC (Tummala et al., 2014) and NASH incidence is

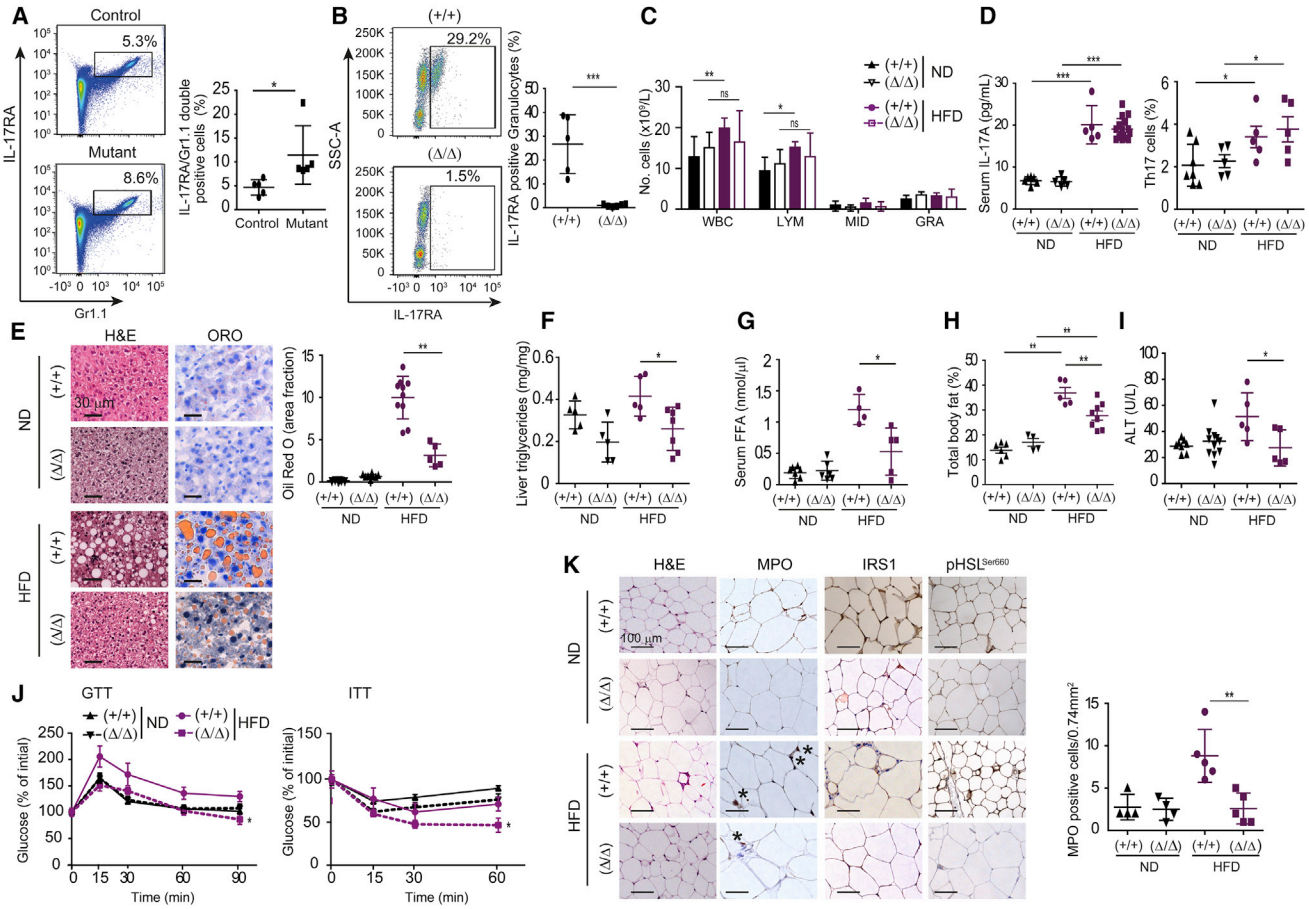

Figure 6. Genetic Ablation of IL-17RA in Myeloid Cells Blocks IL-17A Signaling and Suppresses HFD-Induced IR

(A) Representative flow cytometry of blood from 32-week-old hURI-tetOFF^{hep} mice showing IL-17RA staining in the Gr1.1$^+$ population and quantification of IL-17RA$^+$ cells in the Gr1.1$^+$ population (n ≥ 5).

(B) Representative flow cytometry of blood from 24-week-old IL-17RA (+/+)^{Myeloid} and IL-17RA (Δ/Δ)^{Myeloid} mice showing IL-17RA staining in the Gr1.1$^+$ population and quantification of IL-17RA$^+$ cells in the Gr1.1$^+$ population (n ≥ 5).

(C) Hemogram of 24-week-old IL-17RA (+/+)^{Myeloid} and IL-17RA (Δ/Δ)^{Myeloid} mice under ND or HFD since 8 weeks of age (n ≥ 5).

(D) Circulating IL-17A and quantification of Th17 cells in livers from mice described in (C) (n ≥ 5).

(E) Staining of livers and ORO quantification from mice described in (C) (n ≥ 5).

(F and G) Quantification of hepatic TG (F) and FFA (G) from mice described in (C) (n ≥ 5).

(H) Percentage of body fat in mice described in (C) (n ≥ 5).

(I) ALT in mice described in (C) (n ≥ 5).

(J) GTT and ITT in mice described in (C) (n ≥ 4).

(K) Staining and IHC of WAT and MPO quantification from mice described in (C). Asterisks denote MPO$^+$ cells.

Statistical analysis was performed using two-way ANOVA (J) or unpaired two-tailed Student's t test (A–I and K). Data are represented as means ± SD. *p ≤ 0.05, **p ≤ 0.01, ***p ≤ 0.001. See also Figure S6.

high among patients with chronic viral infections (Blonsky and Harrison, 2008; Nascimento et al., 2012), we also analyzed URI expression and IL-17A levels in human HCC samples with HBV or HCV infection. As we reported previously (Tummala et al., 2014), HCC samples from HBV/HCV-infected patients exhibited elevated URI expression, which correlated positively with IL-17A levels (Figures 8K, S8A, and S8B). However, URI expression did not correlate with IL-17A in HCC from alcoholic steatohepatitis patients (Figure S8C), suggesting that the URI/IL-17A axis may mainly influence NASH-induced HCC.

Moreover, HCC samples but not normal livers presented high levels of IL-17A (Figure 8L), and enhanced IL-17A and IL-17RA correlated positively with URI expression (Figures 8L and S8D). Interestingly, increased IL-17A associated with high URI expression in tumoral tissue was mainly confined to the peritumoral tissue (Figure 8M), suggesting that in human livers, inflammation may contribute to HCC progression through a paracrine signal involving IL-17A. Thus, URI/IL-17A signaling may influence HCC development in NASH-predisposed or hepatitis virus-infected patients.

DISCUSSION

High body mass index increases cancer risks (Arnold et al., 2015). We report here that URI expression-mediated genotoxic

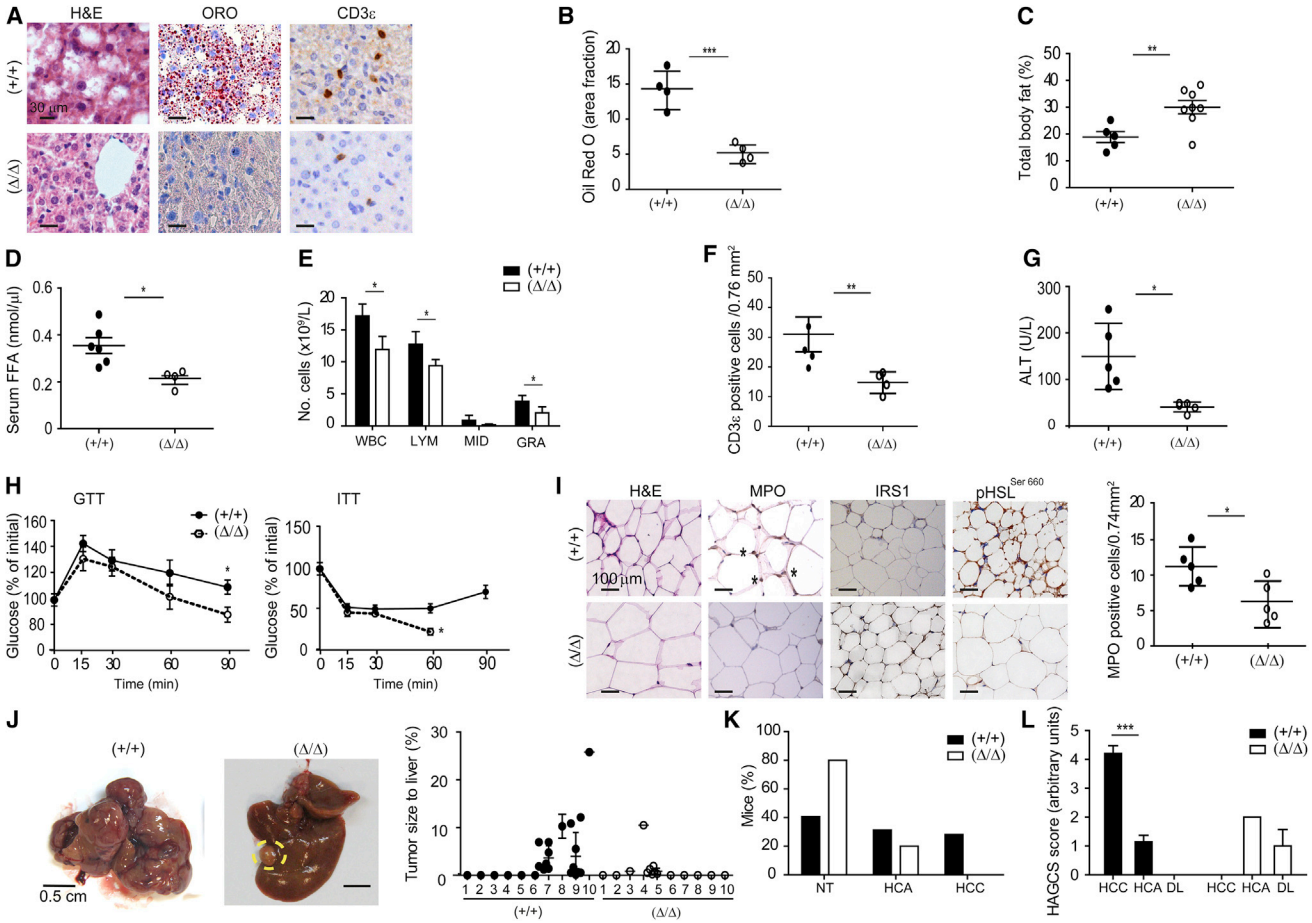

Figure 7. Genetic Ablation of IL-17RA in Myeloid Cells Alleviates IR, NASH, and HCC in Mutants

(A) Staining and IHC of livers from 32-week-old hURI (mutant), IL-17RA $(+/+)^{Myeloid}$ and hURI (mutant), and IL-17RA $(\Delta/\Delta)^{Myeloid}$ mice ($n \geq 4$).

(B) Quantification of hepatic ORO from (A).

(C) Percentage of body fat in mice described in (A) ($n \geq 5$).

(D) FFA in mice described in (A) ($n \geq 4$).

(E) Hemogram of mice described in (A) ($n \geq 4$).

(F) CD3ε quantification from (A).

(G) ALT in mice described in (A) ($n \geq 4$).

(H) GTT and ITT in mice described in (A) ($n \geq 6$).

(I) Staining and IHC of WAT and MPO quantification from mice described in (A) ($n \geq 5$). Asterisks denote MPO^{+} cells.

(J) Representative pictures of livers and quantification of tumoral area ($n \geq 10$) from 65-week-old hURI (mutant), IL-17RA $(+/+)^{Myeloid}$ and hURI (mutant), and IL-17RA $(\Delta/\Delta)^{Myeloid}$ mice. Dashed yellow circles denote tumors.

(K) Percentage of mice described in (J) bearing liver abnormalities.

(L) HAGCS score in mice described in (J) ($n \geq 5$). DL, dysplastic lesions.

Statistical analysis was performed using two-way ANOVA (H, right panel) or unpaired two-tailed Student's t test (B–G, H [left panel], I, and L). Data are represented as means ± SD. *$p \leq 0.05$, **$p \leq 0.05$, ***$p \leq 0.001$. See also Figure S7.

stress is apparently the initiating event in nutrient excess-induced NASH and HCC development by mobilizing Th17 cells and increasing IL-17A levels.

IL-17A induces WAT neutrophil infiltration, IR and lipolysis causing NASH, and HCC. Metabolic inflammation-induced IR leads to hepatic fat accumulation; therefore, it is not steatosis that causes IR. In fact, inflammation precedes steatosis in different models of human NASH (Wolf et al., 2014; Zhao et al., 2015) and FA uptake in the liver due to WAT IR accounts for almost two-thirds of lipid accumulation in NASH patients (Donnelly et al., 2005). Therefore, the hURI-tetOFF^{hep} mouse recapitulates all histopathological features of NASH: inflammation, hepatic steatosis with Mallory-Denk bodies, steatosis, fibrosis, and liver injury. All of these events are of great importance to pathologically define the presence of NASH, the development of which does not strictly follow the "two-hit" hypothesis (Day and James, 1998). Notably, the incidence of hepatocarcinogenesis is higher in the hURI-tetOFF^{hep} mice than in the HFD model (Tummala et al., 2014; Wolf et al., 2014) and seems to be proportional to the Th17 cell counts. Levels of Th17 cells may thus account for promoting NASH-induced HCC, whereas high steatosis observed in the HFD-treated mice is apparently a

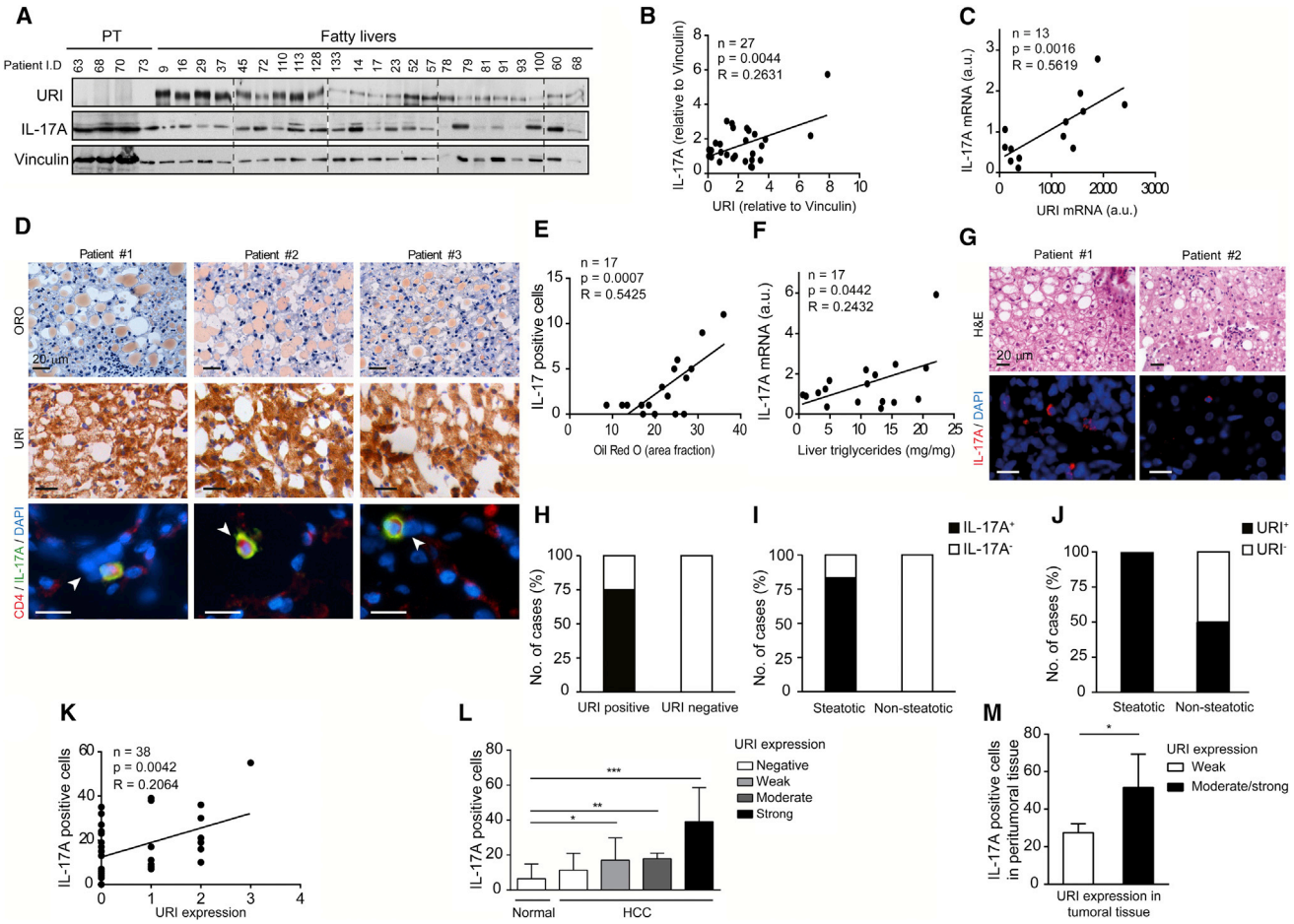

Figure 8. IL-17A Levels in Human Hepatitis, Human Fatty Livers, and Viral Hepatitis-Associated Human HCC Correlate Positively with Steatosis and URI Expression

(A) WB in human peritumoral (n = 4) and fatty livers (n = 23). Dotted lines indicate the different membranes, from the same film and exposure.
(B) Linear regression of hepatic of URI and IL-17A levels from (A) (n = 27).
(C) Linear regression of hepatic URI and IL-17A mRNA levels in human fatty livers (n = 13).
(D) Staining, IHC, and immunofluorescence in liver sections from human obese individuals. Arrowheads denote $CD4^+IL\text{-}17A^+$ cells.
(E) Linear regression of $IL\text{-}17A^+$ cells and ORO staining from (D) (n = 17).
(F) Linear regression of hepatic IL-17A mRNA levels and hepatic TG in human obese individuals (n = 17).
(G) H&E staining and immunofluorescence in livers from human HCV/HBV samples ($n \geq 5$).
(H) Percentage of cases with presence of $IL\text{-}17A^+$ cells in URI^+ versus URI^- human HCV patients ($n \geq 5$).
(I) Percentage of cases with presence of $IL\text{-}17A^+$ cells in steatotic versus non-steatotic human HCV patients ($n \geq 5$).
(J) Percentage of cases positive for URI in steatotic versus non-steatotic human HCV patients ($n \geq 5$).
(K) Linear regression of hepatic URI and IL-17A levels in human HCC from HBV and HCV patients in tissue microarrays (n = 38).
(L) Stratification of human samples according to URI and IL-17A expression in normal and HCC (n = 97).
(M) Stratification of human samples according to IL-17A peritumoral levels and URI tumoral levels (n = 21).
Statistical analysis was performed using unpaired two-tailed Student's t test (L and M) and linear regression (B, C, E, F, and K). Data are represented as means ± SD. $^*p \leq 0.05$, $^{**}p \leq 0.05$, $^{***}p \leq 0.001$. See also Figure S8.

consequence of overfeeding. Thus, hepatic URI expression induced by nutrient overload leads to increased DNA damage, which is the driving force in NASH-induced HCC. Hence, the hURI-tetOFF^{hep} mouse mimics nutrient overload and is a model of NASH-induced HCC.

Blocking IL-17A signaling reduces steatosis and liver injury, and prevents HCC. Surprisingly, steatosis arises after dysplastic lesions, which appear when significant inflammation is observed (at 8 weeks of age). Thus, liver fat deposits may fuel and facilitate survival of transformed cells and progression of dysplastic lesions promoting HCC. Abolishing steatosis also alleviates liver injury. Importantly, hepatic ALT levels increase at the time of lipid accumulation (at 32 weeks of age) rather than immediately after inflammatory cell infiltration (at 8 weeks of age) (Tummala et al., 2014). Thus, chronic liver injury apparently depends on steatosis. In fact the progression of liver injury in time may be due to the complex interactions between hepatic inflammation, IR, and steatosis, via unknown mechanisms that may implicate the hepatic stellate cells' cytokines. Hence, T2D and IR may be risk factors for NASH and HCC development (Gruben et al.,

2014; Nagle et al., 2009; Perry et al., 2014). Blocking IL-17A may therefore be useful for preventing NASH-induced IR and associated hepatocarcinogenesis.

IR is also linked to inflammatory diseases associated with IL-17A, e.g., HVB/HVC, corroborating the close relationship between metabolism and immune responses (Gregor and Hotamisligil, 2011). Patients with chronic viral hepatitis exhibit high NASH prevalence (Blonsky and Harrison, 2008; Nascimento et al., 2012). NASH risk factors and effects on patients with HCV or HBV are largely unknown because histological criteria used to diagnose NASH are ambiguous (predominantly perisinusoidal fibrosis and clarification/ballooning of liver cells, both observed in the URI mouse model). HCV patients with NASH exhibit elevated body mass index, serum glucose and TG levels, and high frequencies of diabetes and metabolic syndrome (Blonsky and Harrison, 2008). Interestingly, IL-17A-expressing Th17 cells are induced in HCV patients (Rowan et al., 2008), suggesting that IL-17A is central to HCV-associated metabolic and hepatic dysfunctions. Notably, URI expression is modulated by HBV/HCV infection and inflammatory cues (Tummala et al., 2014). In line with the fact that IL-17RA may be expressed in the liver (Lafdil et al., 2010), rIL-17A also enhances URI expression in hepatocytes, inducing DNA damage and increased Th17 cells. Thus, increased IL-17A may act as a positive feedback loop to enhance URI expression in hepatocytes strengthening genotoxic stress and IL-17A levels. Thus, our data suggest that URI-induced IL-17A may also be central to viral infection- or inflammation-associated metabolic and hepatic dysfunctions. Treatment of HCV represents a socio-economic challenge of our society, in that blocking IL-17A or Th17 cell differentiation with digoxin may provide effective and inexpensive prophylaxis for HBV- or HCV-infected patients with high NASH and HCC risks.

Digoxin may also inhibit RORγt transcriptional activity in innate lymphoid cells 3 (ILC3) and thus suppress IL-17A in ILC3 cells. However, it remains to be determined whether ILC3 plays a role in the pathology of NASH-induced HCC. Digoxin also inhibits hypoxia-inducible factor 1α (HIF-1α) synthesis and blocks tumor growth (Zhang et al., 2008), but there is no clear evidence for HIF-1α functions in NASH and, in our model, digoxin unlikely acts on HIF-1α since no increase of HIF-1α is detected in URI mutant livers (not shown).

Our data indicate that hepatic URI expression is the molecular mediator linking nutrients' excess to genotoxic stress, Th17 infiltration, IL-17A production, and metabolic dysfunction-associated IR, which causes hepatic fat accumulation and HCC. Thus, blocking IL-17A signaling may be effective for preventing NASH and hepatocarcinogenesis, especially in patients with high hepatic URI expression, genotoxic stress, and/or early signs of diabetes. Finally, IL-17A could be potentially a valuable non-invasive marker of IR and NASH pathogenesis in obese patients.

EXPERIMENTAL PROCEDURES

Generation and Handling of Mice

hURI-tetOFF^{hep} and URI(+/Δ)^{hep} mice were generated as recently reported (Tummala et al., 2014). LysM-Cre and IL-17RA conditional knockout mice were previously described (Clausen et al., 1999; El Malki et al., 2013). Deletion of IL-17RA in the myeloid lineage was obtained by crossing *Il17ra*-flox mouse with LysM-Cre line, and was confirmed by genotyping and flow cytometry. All mice were housed in pathogen-free conditions. All experiments were approved by the CNIO-ISCIII Ethics Committee and performed in accordance with the guidelines for ethical conduct in the care and use of animals as stated in the international guiding principles for biomedical research involving animals, developed by the Council for International Organizations of Medical Sciences. Littermates were always used as controls.

Mouse Diets and Treatments

Mice were fed either with chow diet (here termed normal diet, ND) (18% fat, 58% carbohydrates, and 24% proteins) (Harlan Laboratories, 2018S), HFD (45% fat, 35% carbohydrates, and 20% proteins) (Research Diets, D12451), CD-HFD (60% fat, 20% carbohydrates, and 20% proteins) (Research Diets, D05010403), MCD-HFD (62% fat, 20% carbohydrates, and 18% proteins) (Research Diets, A06071301B), DOX (15% kcal fat and 2,000 ppm doxycycline, which represents in the daily diet an estimated dose of 0.36 mmol/kg) (Research Diets, D12100402i), or tamoxifen (tamoxifen citrate 400 ppm) (Research Diets, TD.55125). Food and water were provided ad libitum.

For DEN treatment, 14-day-old C57BL/6 mice were intraperitoneally injected with 25 mg/kg DEN (Sigma, N0258) or injected with DEN and fed with HFD at 8 weeks of age.

For rIL-17A treatment, 4-week-old C57BL/6 mice were intraperitoneally injected with 0.5 μg/mouse of recombinant mouse IL-17A (GenScript, Z03031-50) three times per week for a period of 4 weeks.

For anti-IL-17A treatment, 8-week-old hURI-tetOFF^{hep} mice were intraperitoneally injected with 100 μg/mouse (1 mg/ml) of anti-IL-17A (R&D, MAB421, clone 50104) every other day until the age of 32 weeks.

For digoxin treatment, 8-week-old hURI-tetOFF^{hep} or DEN-HFD-fed C57BL/6 mice were treated with digoxin (Sigma, D6770) dissolved in the drinking water (30 μg/ml) until 32 weeks of age. Drinking treatment was changed daily. NR (97% purity, Waterstonetech Pharma) was administered as previously described (Tummala et al., 2014).

Tumor Quantification

Macroscopically visible tumors were measured as previously described (Tummala et al., 2014).

Glucose and Insulin Tolerance Testing

Mice were fasted for 6 hr and injected intraperitoneally with 2 g/kg glucose in water (GTT) or 0.75 U/kg insulin in 0.9% NaCl (ITT) (Sun et al., 2006; Um et al., 2004). Blood from the tail vein was obtained before the injection and at 15, 30, 60, and 90 min after the injection for determination of blood glucose using Accu-Check Compact test strips (Roche, 13072).

Total Body Fat Measurement

Animals were anesthetized with isoflurane (Isovet, Braun Vetcare) and densitometry was assessed by a densitometer (Piximus, Lunar Corporation). Percentage of body fat was quantified using Lunar PIXImus 2.10 software.

Blood Parameters

Blood parameters were measured as detailed in Supplemental Experimental Procedures. In brief, blood was collected from the heart and transferred to an EDTA-containing tube for hemogram analysis using Abacus Junior Vet analyzer (Diatrom). Plasma was collected after centrifugation at 1,500 rpm and 4°C for 15 min, and kept at −80°C until further analysis. Different blood parameters were measured using kits from different manufacturers.

Triglyceride Extraction and Quantification

TGs were extracted from 20–30 mg of livers and quantified using a TG Colorimetric Assay Kit (Cayman Chemical, 10010303) according to the manufacturer's instructions.

Mononuclear Cell Isolation

Inflammatory cell isolation was performed as detailed in Supplemental Experimental Procedures. In brief, liver or visceral fat was excised and minced in RMPI 1640 media supplemented with 10% fetal bovine serum (cell buffer). The resulting suspension was mashed through a mesh and after centrifugation erythrocytes were removed with red blood cell lysis buffer. For isolation of liver inflammatory cells, after centrifugation the pellet was resuspended in 38%

Percoll in cell buffer and underlaid with 70% Percoll in PBS, and further centrifuged at 500 × *g* for 30 min at 4°C. Interface with mononuclear cells was collected and washed with cell buffer. After a short centrifugation, the pellet was washed and finally resuspended in 5% BSA and 2 mM EDTA in Ca^{2+}/Mg^{2+}-free PBS (MACS buffer). After centrifugation the pellet was resuspended in MACS buffer to isolate macrophages from WAT.

Flow Cytometry

Flow cytometry was performed as detailed in Supplemental Experimental Procedures. In brief, cells were resuspended in MACS buffer containing Mouse BD Fc block (BD Biosciences, 553141). Following washing with MACS buffer, cells were stained for cell death discriminator and different markers. For liver mononuclear staining, T cell receptors were stimulated. After washing, cells were resuspended and analyzed using FACS Canto II (BD Biosciences) or LSR Fortessa (BD Biosciences).

Human Samples

Human samples were obtained from the CNIO Biobank. Analysis of human samples was approved by the Research Ethics and Animal Welfare Committee from the Institute of Health Carlos III (ISCIII), and informed consent was obtained from all subjects.

Statistical Analysis

Statistical analyses were performed using GraphPad Prism V5.0 software. Statistical significance (*$p \leq 0.05$, **$p \leq 0.01$, and ***$p \leq 0.001$) between the means of a minimum of three groups was determined using unpaired two-tailed Student's t test, two-way ANOVA, or linear regression analysis. Results are expressed as the mean value ± SD. All results are representative of at least three independent experiments.

SUPPLEMENTAL INFORMATION

Supplemental Information includes Supplemental Experimental Procedures and eight figures and can be found with this article online at http://dx.doi.org/10.1016/j.ccell.2016.05.020.

AUTHOR CONTRIBUTIONS

A.L.G. and A.T. designed and performed most of the experiments. A.L.G. started and developed the project. A.T. continued the project and revised the manuscript. S.B. performed most of WAT WB. K.S.T. and N.D. engineered the hURI-tetOFF^{hep} mouse and created the HAGCS score. M.Y. and N.D. engineered the URI conditional knockout mouse. A.W. provided the *Il17ra*-flox mouse. J.P.T. shared observations on URI expression in HCCs and its association to hepatitis viral infections. C.P. analyzed histopathologically mouse and human tissues and determined the HAGCS score. A.L.G., A.T., and N.D. analyzed all the data. N.D. designed the experiments, conceived the project, and secured funding. N.D. wrote the manuscript with A.L.G. and A.T.

ACKNOWLEDGMENTS

We thank the CNIO Biobank (M.J. Artiga and M. Morente) and Biobanco La Fe for collecting livers derived from obese patients and associated data used in this study. We are grateful to M. Rodriguez-Justo for analyzing some human HCCs as previously reported (Tummala et al., 2014) and to E. Wagner for critical reading of the manuscript. We are grateful to W. Krek for sharing URI antibodies previously reported (Tummala et al., 2014). We are thankful to the CNIO and the CCB program for sharing some reagents. A.L.G. was a recipient of the Caja Navarra postdoctoral fellowship. N.D. is a recipient of the Spanish Ramón y Cajal fellowship. This work was supported by the CNIO-Severo Ochoa, the Spanish Ministry of Economy and Competitiveness (SAF2010 - 18518 and SAF2013-46089-R), EFSD and WCR (AICR - 11-0242).

Received: May 12, 2015
Revised: May 15, 2016
Accepted: May 28, 2016
Published: July 11, 2016

REFERENCES

Arnold, M., Pandeya, N., Byrnes, G., Renehan, A.G., Stevens, G.A., Ezzati, M., Ferlay, J., Miranda, J.J., Romieu, I., Dikshit, R., et al. (2015). Global burden of cancer attributable to high body-mass index in 2012: a population-based study. Lancet Oncol. *16*, 36–46.

Bjornsson, E., Lindberg, J., and Olsson, R. (1997). Liver reactions to oral low-dose tetracyclines. Scand. J. Gastroenterol. *32*, 390–395.

Blonsky, J.J., and Harrison, S.A. (2008). Review article: nonalcoholic fatty liver disease and hepatitis C virus—partners in crime. Aliment. Pharmacol. Ther. *27*, 855–865.

Clausen, B.E., Burkhardt, C., Reith, W., Renkawitz, R., and Forster, I. (1999). Conditional gene targeting in macrophages and granulocytes using LysMcre mice. Transgenic Res. *8*, 265–277.

Day, C.P., and James, O.F. (1998). Steatohepatitis: a tale of two "hits"? Gastroenterology *114*, 842–845.

Deboyser, D., Goethals, F., Krack, G., and Roberfroid, M. (1989). Investigation into the mechanism of tetracycline-induced steatosis: study in isolated hepatocytes. Toxicol. Appl. Pharmacol. *97*, 473–479.

Di Tommaso, L., Franchi, G., Park, Y.N., Fiamengo, B., Destro, A., Morenghi, E., Montorsi, M., Torzilli, G., Tommasini, M., Terracciano, L., et al. (2007). Diagnostic value of HSP70, glypican 3, and glutamine synthetase in hepatocellular nodules in cirrhosis. Hepatology *45*, 725–734.

Donath, M.Y., Schumann, D.M., Faulenbach, M., Ellingsgaard, H., Perren, A., and Ehses, J.A. (2008). Islet inflammation in type 2 diabetes: from metabolic stress to therapy. Diabetes Care *31* (*Suppl 2*), S161–S164.

Donnelly, K.L., Smith, C.I., Schwarzenberg, S.J., Jessurun, J., Boldt, M.D., and Parks, E.J. (2005). Sources of fatty acids stored in liver and secreted via lipoproteins in patients with nonalcoholic fatty liver disease. J. Clin. Invest. *115*, 1343–1351.

El Malki, K., Karbach, S.H., Huppert, J., Zayoud, M., Reissig, S., Schuler, R., Nikolaev, A., Karram, K., Munzel, T., Kuhlmann, C.R., et al. (2013). An alternative pathway of imiquimod-induced psoriasis-like skin inflammation in the absence of interleukin-17 receptor a signaling. J. Invest. Dermatol. *133*, 441–451.

Fossiez, F., Djossou, O., Chomarat, P., Flores-Romo, L., Ait-Yahia, S., Maat, C., Pin, J.J., Garrone, P., Garcia, E., Saeland, S., et al. (1996). T cell interleukin-17 induces stromal cells to produce proinflammatory and hematopoietic cytokines. J. Exp. Med. *183*, 2593–2603.

Gregor, M.F., and Hotamisligil, G.S. (2011). Inflammatory mechanisms in obesity. Annu. Rev. Immunol. *29*, 415–445.

Gruben, N., Shiri-Sverdlov, R., Koonen, D.P., and Hofker, M.H. (2014). Nonalcoholic fatty liver disease: a main driver of insulin resistance or a dangerous liaison? Biochim. Biophys. Acta *1842*, 2329–2343.

Guo, X., Xiong, L., Sun, T., Peng, R., Zou, L., Zhu, H., Zhang, J., Li, H., and Zhao, J. (2012). Expression features of SOX9 associate with tumor progression and poor prognosis of hepatocellular carcinoma. Diagn. Pathol. *7*, 44.

Harley, I.T., Stankiewicz, T.E., Giles, D.A., Softic, S., Flick, L.M., Cappelletti, M., Sheridan, R., Xanthakos, S.A., Steinbrecher, K.A., Sartor, R.B., et al. (2014). IL-17 signaling accelerates the progression of nonalcoholic fatty liver disease in mice. Hepatology *59*, 1830–1839.

He, G., Yu, G.Y., Temkin, V., Ogata, H., Kuntzen, C., Sakurai, T., Sieghart, W., Peck-Radosavljevic, M., Leffert, H.L., and Karin, M. (2010). Hepatocyte IKKbeta/NF-kappaB inhibits tumor promotion and progression by preventing oxidative stress-driven STAT3 activation. Cancer Cell *17*, 286–297.

He, G., Dhar, D., Nakagawa, H., Font-Burgada, J., Ogata, H., Jiang, Y., Shalapour, S., Seki, E., Yost, S.E., Jepsen, K., et al. (2013). Identification of liver cancer progenitors whose malignant progression depends on autocrine IL-6 signaling. Cell *155*, 384–396.

Huh, J.R., Leung, M.W., Huang, P., Ryan, D.A., Krout, M.R., Malapaka, R.R., Chow, J., Manel, N., Ciofani, M., Kim, S.V., et al. (2011). Digoxin and its derivatives suppress TH17 cell differentiation by antagonizing RORgammat activity. Nature *472*, 486–490.

Korn, T., Bettelli, E., Oukka, M., and Kuchroo, V.K. (2009). IL-17 and Th17 cells. Annu. Rev. Immunol. *27*, 485–517.

Lafdil, F., Miller, A.M., Ki, S.H., and Gao, B. (2010). Th17 cells and their associated cytokines in liver diseases. Cell Mol. Immunol. *7*, 250–254.

Lo, R.C., and Ng, I.O. (2013). Hepatocellular tumors: immunohistochemical analyses for classification and prognostication. Chin. J. Cancer Res. *23*, 245–253.

Marengo, A., Rosso, C., and Bugianesi, E. (2016). Liver cancer: connections with obesity, fatty liver, and cirrhosis. Annu. Rev. Med. *67*, 103–117.

Miyamoto, M., Prause, O., Sjostrand, M., Laan, M., Lotvall, J., and Linden, A. (2003). Endogenous IL-17 as a mediator of neutrophil recruitment caused by endotoxin exposure in mouse airways. J. Immunol. *170*, 4665–4672.

Mraz, M., and Haluzik, M. (2014). The role of adipose tissue immune cells in obesity and low-grade inflammation. J. Endocrinol. *222*, R113–R127.

Nagle, C.A., Klett, E.L., and Coleman, R.A. (2009). Hepatic triacylglycerol accumulation and insulin resistance. J. Lipid Res. *50* (*Suppl*), S74–S79.

Nascimento, A.C., Maia, D.R., Neto, S.M., Lima, E.M., Twycross, M., Baquette, R.F., and Lobato, C.M. (2012). Nonalcoholic fatty liver disease in chronic hepatitis B and C patients from Western Amazon. Int. J. Hepatol. *2012*, 695950.

Osada, T., Nagashima, I., Tsuno, N.H., Kitayama, J., and Nagawa, H. (2000). Prognostic significance of glutamine synthetase expression in unifocal advanced hepatocellular carcinoma. J. Hepatol. *33*, 247–253.

Park, E.J., Lee, J.H., Yu, G.Y., He, G., Ali, S.R., Holzer, R.G., Osterreicher, C.H., Takahashi, H., and Karin, M. (2010). Dietary and genetic obesity promote liver inflammation and tumorigenesis by enhancing IL-6 and TNF expression. Cell *140*, 197–208.

Patel, P.S., Buras, E.D., and Balasubramanyam, A. (2013). The role of the immune system in obesity and insulin resistance. J. Obes. *2013*, 616193.

Perry, R.J., Samuel, V.T., Petersen, K.F., and Shulman, G.I. (2014). The role of hepatic lipids in hepatic insulin resistance and type 2 diabetes. Nature *510*, 84–91.

Rowan, A.G., Fletcher, J.M., Ryan, E.J., Moran, B., Hegarty, J.E., O'Farrelly, C., and Mills, K.H. (2008). Hepatitis C virus-specific Th17 cells are suppressed by virus-induced TGF-beta. J. Immunol. *181*, 4485–4494.

Sadik, C.D., Kim, N.D., and Luster, A.D. (2011). Neutrophils cascading their way to inflammation. Trends Immunol. *32*, 452–460.

Sun, Y., Asnicar, M., Saha, P.K., Chan, L., and Smith, R.G. (2006). Ablation of ghrelin improves the diabetic but not obese phenotype of ob/ob mice. Cell Metab. *3*, 379–386.

Takahashi, Y., Soejima, Y., and Fukusato, T. (2012). Animal models of nonalcoholic fatty liver disease/nonalcoholic steatohepatitis. World J. Gastroenterol. *18*, 2300–2308.

Talukdar, S., Oh da, Y., Bandyopadhyay, G., Li, D., Xu, J., McNelis, J., Lu, M., Li, P., Yan, Q., Zhu, Y., et al. (2012). Neutrophils mediate insulin resistance in mice fed a high-fat diet through secreted elastase. Nat. Med. *18*, 1407–1412.

Tilg, H., and Moschen, A.R. (2010). Evolution of inflammation in nonalcoholic fatty liver disease: the multiple parallel hits hypothesis. Hepatology *52*, 1836–1846.

Tummala, K.S., Gomes, A.L., Yilmaz, M., Grana, O., Bakiri, L., Ruppen, I., Ximenez-Embun, P., Sheshappanavar, V., Rodriguez-Justo, M., Pisano, D.G., et al. (2014). Inhibition of de novo NAD(+) synthesis by oncogenic uri causes liver tumorigenesis through DNA damage. Cancer Cell *26*, 826–839.

Uenishi, T., Kubo, S., Yamamoto, T., Shuto, T., Ogawa, M., Tanaka, H., Tanaka, S., Kaneda, K., and Hirohashi, K. (2003). Cytokeratin 19 expression in hepatocellular carcinoma predicts early postoperative recurrence. Cancer Sci. *94*, 851–857.

Um, S.H., Frigerio, F., Watanabe, M., Picard, F., Joaquin, M., Sticker, M., Fumagalli, S., Allegrini, P.R., Kozma, S.C., Auwerx, J., and Thomas, G. (2004). Absence of S6K1 protects against age- and diet-induced obesity while enhancing insulin sensitivity. Nature *431*, 200–205.

Wolf, M.J., Adili, A., Piotrowitz, K., Abdullah, Z., Boege, Y., Stemmer, K., Ringelhan, M., Simonavicius, N., Egger, M., Wohlleber, D., et al. (2014). Metabolic activation of intrahepatic CD8(+) T cells and NKT cells causes nonalcoholic steatohepatitis and liver cancer via cross-talk with hepatocytes. Cancer Cell *26*, 549–564.

Zhang, H., Qian, D.Z., Tan, Y.S., Lee, K., Gao, P., Ren, Y.R., Rey, S., Hammers, H., Chang, D., Pili, R., et al. (2008). Digoxin and other cardiac glycosides inhibit HIF-1alpha synthesis and block tumor growth. Proc. Natl. Acad. Sci. USA *105*, 19579–19586.

Zhao, Y.J., Ju, Q., and Li, G.C. (2013). Tumor markers for hepatocellular carcinoma. Mol. Clin. Oncol. *1*, 593–598.

Zhao, L., Zhong, S., Qu, H., Xie, Y., Cao, Z., Li, Q., Yang, P., Varghese, Z., Moorhead, J.F., Chen, Y., and Ruan, X.Z. (2015). Chronic inflammation aggravates metabolic disorders of hepatic fatty acids in high-fat diet-induced obese mice. Sci. Rep. *5*, 10222.